CFD analysis of industrial multi-staged stirred vessels

Marion Alliet-Gaubert [a,*], Rodolphe Sardeing [a], Catherine Xuereb [a], Philippe Hobbes [b], Bertrand Letellier [c], Philippe Swaels [d]

[a] *Laboratoire de Génie Chimique UMR 5503 CNRS/INPT/UPS, 5 Rue Paulin Talabot, B.P. 1301, 31106 Toulouse Cedex 1, France*
[b] *INSA de Rouen, Place Emile Blondel, B.P. 8, 76131 Mont Saint Aignan Cedex, France*
[c] *Cray Valley—Total, La Défense, 12, place de l'Iris, 92062 Paris La Défence Cedex, France*
[d] *Cray Valley, Centre de recherche de l'Oise, BP 22, Parc technologique Alata, 60550 Verneuil en Halatte, France*

Abstract

This paper presents tools for analysis of CFD results adapted for flows in multi-stage stirred vessels through out two industrial cases. Those tanks fitted with double-flow impellers are used first to cool down highly viscous resins and subsequently for indirect emulsification. Since the simulation of these processes in their whole complexity would be unrealistic, it considers single-phase flows without heat transfer. The result analysis in order to prove that the mixing and the circulation are effective is not usual; in these cases, the circulation and impeller numbers are not adapted. The average axial flow numbers are relevant of the circulation in the whole tank and of the connection between the flows produced by the propellers in the given configuration. The velocity profiles give relevant results, but are not sufficient whereas the particle tracking validates that the propellers do not work together in one case and do work together in a second one.

Keywords: CFD; Multiple impellers; Stirred vessel; Viscous mixing; Transient flow; Industrial application; Double flux impeller

1. Introduction

The progress of computer fluid dynamics (CFD) for the last 20 years has made it an important tool for process hydrodynamic understanding in stirred tanks. In a state-of-the-art in CFD simulation of stirred vessel, Sommerfeld and Decker [1] conclude that single-phase simulation with the Reynolds Average Navier–Stockes equations (RANS) and standard k–ε turbulence model can predict the mean velocities of a turbulent flow in a stirred vessel. An accurate prediction of turbulent properties requires more precise grid, or even the use of large eddy simulation (LES) or direct numerical simulation (DNS). The simulation of two-phase flows using an Euler/Euler approach requires not only much CPU time, but also reliable models of physical phenomena such as break-up and coalescence, which need to be improved to represent the actual physical phenomena. On the other hand, the Euler/Lagrange approach allows for a very detailed modelling of the physical phenomena occurring on the scale of the particle, but convergence problems limit its application to smaller volume fraction of the dispersed phase [1]. Some fields of study which are not investigated in the previously quoted state of the art [1], like laminar flows, flows combined with heat transfer or flow combined with reaction, give interesting results. The modelling of laminar flow is a priori rather simple since no closure equation is needed. For example, the works of Thibault and Tanguy [2] or Letellier et al. [3] show a good agreement between experimental and numerical evolution of power number as a function of Reynolds number. The difficulty of modelling these systems may come from possible non-Newtonian rheology (see, for example, [2] or [4]). Zakrzewska and Jaworski's [5] recent study of a static heat transfer system, separating the solution of heat transfer equations from the solution of RANS equations, led to good agreement on local heat transfer coefficients. Brucato et al. [6] show that CFD used as a support of single-phase reactions gives good results when micromixing is negligible.

The industrial systems that need advanced study are often complex cases requiring complex models and a lot of CPU time and memory. Before implementing complex modelling, it is worth to use CFD tools with modelling simplifications.

* Corresponding author. Tel.: +33 5 34 61 52 41; fax: +33 5 34 61 52 53.
E-mail address: Marion.AllietGaubert@ensiacet.fr (M. Alliet-Gaubert).

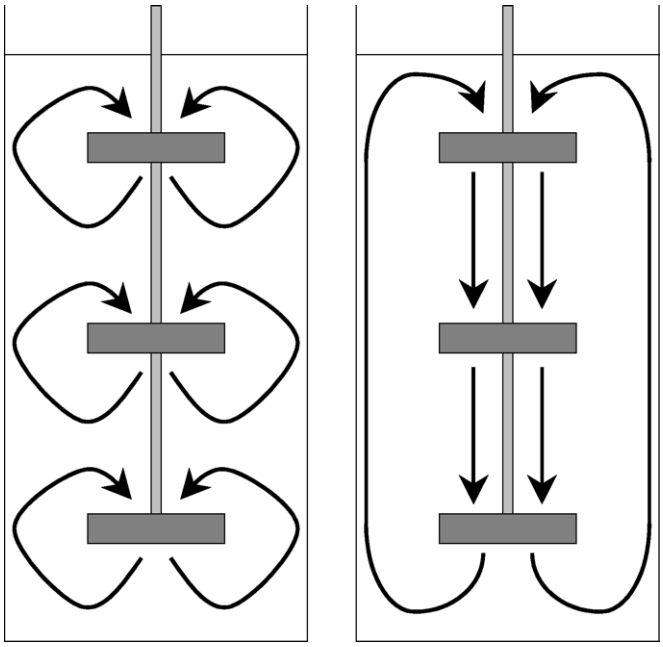

Fig. 1. Two idealised circulation profiles in multistage stirred vessels.

However, this should be done with the utmost care not only in the modelling but also in the results analyses. This last point is going to be presented in this article.

The analysis of CFD results is generally not so easy due to the huge amount of data: several values by cells, and up to 13 million cells for a simulation [7], which can be multiplied by the number of time steps, when the simulation is time dependent.

Stirred vessels simulations present an additional complexity since they are fully three-dimensional: the biggest velocity component is tangential and circulation is significant in the three directions. For analysis of CFD results of stirred vessels, dimensional reduction, neglecting one dimension from the others, should be done carefully.

This study concerns an industrial multi-stage agitated tanks used first to cool down highly viscous resins like epoxy or polyester (alkyd resins) and subsequently for indirect emulsification (phase inversion process). This article focuses on the most critical points of the process, considering the bulk as pseudohomogeneous (i.e. constant density and viscosity). The rather low Reynolds numbers, in between 60 and 173, specify that the flows are in the transient regime. The objective of this study is to distinguish if the mixing in different tank configurations allows a good heat transfer and a good mixing with the added second phase. For this purpose CFD simulation tools are used.

Stirred vessels with multiple impellers are more often used for liquid–gas mixing [8–10], solid suspensions [11–13], heat transfer [14] or the mixing of viscous fluids [15,3]. For those vessels, there are several circulation profiles in between the two idealised profiles (Fig. 1):

- the movement of each impeller has an influence on a zone restricted to the impeller surrounding (self-feeding), and there is no interaction between loops;
- the movement of each impeller contributes to a global circulation in the vessel.

The mixing is much better for this second case, which may require much power to obtain, especially with viscous liquids. Connected loops are often more efficient considering the mixing. The question is: how can we establish that loops are connected?

This paper begins with the presentation of tools and methods for flow characterisation, followed by two examples of their industrial application.

2. Flow characterization tools and methods

Various methods for results analysis to get a good mixing characterisation have been collected and their fields of application have been specified. The first group concerns macro-indicators such as power number, circulation number, impeller flow number, axial flow number and agitation index. The second group presents local indicators such as velocity profiles, streamlines and particles tracking. Statistical methods such as probability density function of stretching [21] are not treated in this paper. Since they are based on statistic concepts, they need much computer time to be effective. Moreover, they seem well adapted for flow understanding but the understanding at the process level and the comparison of two cases are not direct. For these two reasons, we think they are not yet adapted to handle industrial examples.

2.1. Power and power number

The interest of power calculation is to evaluate energy consumption and its economic impact. Power consumption used for mixing, P, may be calculated using two methods.

The first one integrates the viscous dissipation energy, Φ_V, into the whole bulk volume:

$$P = \iiint_V \eta \Phi_V \, dV \tag{1}$$

where η is the apparent fluid viscosity (Pa s). For an incompressible Newtonian fluid, Φ_V is written:

$$\Phi_V = 2\left[\left(\frac{dv_x}{dx}\right)^2 + \left(\frac{dv_y}{dy}\right)^2 + \left(\frac{dv_z}{dz}\right)^2\right] + \left[\frac{dv_x}{dy} + \frac{dv_y}{dx}\right]^2 + \left[\frac{dv_y}{dz} + \frac{dv_z}{dy}\right]^2 + \left[\frac{dv_x}{dz} + \frac{dv_z}{dx}\right]^2 \tag{2}$$

The second methodology uses the torque, C, applied on the agitation system as given in Eq. (3). With this second method, the power may be calculated for each impeller:

$$P = 2\pi NC \tag{3}$$

where N is the impeller rotational speed.

Power consumption is dimensionless represented by power number, P_0:

$$P_0 = \frac{P}{\rho N^3 D^5} \tag{4}$$

where D is the impeller diameter (m). For single-phase Newtonian fluid, the Reynolds number is defined as:

$$Re = \frac{\rho N D^2}{\mu} \tag{5}$$

where ρ is the liquid density (kg m^{-3}).

In laminar flows, $P_0 Re$ is considered as constant whereas in turbulent flows, P_0 is almost constant.

2.2. Circulation, impeller flow and axial flow numbers

2.2.1. Impeller flow number

The pumping flow rate, Q_{Fl}, corresponds to the fluid flow that is discharged from the impeller swept volume [16]. For an impeller diameter, D, a general expression for calculating the pumping flow is:

$$Q_{\mathrm{Fl}} = \int_{z^-}^{z^+} \pi D \left|(v_r^{\mathrm{o}})_{r=r^+}\right| \,\mathrm{d}z + \int_0^{r^+} 2\pi r \left|(v_z^{\mathrm{o}})_{z=z^+}\right| \,\mathrm{d}r + \int_0^{r^+} 2\pi r \left|(v_z^{\mathrm{o}})_{z=z^-}\right| \,\mathrm{d}r \tag{6}$$

where z^+, z^- and r^+ are the boundaries of the impeller swept volume and the superscript 'o' refers to the fluid moving out of this volume.

In order to compare different agitators operating in different conditions, the discharge flow rate of the impeller may be expressed as the dimensionless pumping number by normalizing Q_{Fl} by ND^3:

$$\mathrm{Fl} = \frac{Q_{\mathrm{Fl}}}{ND^3} \tag{7}$$

In turbulent flows, Fl is considered as constant.

2.2.2. Circulation time and flow rate

Circulation time, t_{C}, is known as the time for a fluid element to cover the entire volume, V, of the tank. It is measured using the time period between two subsequent concentration peaks of a tracer [17]. It is specified as satisfactory if working with helical agitator but not so when radial discharge flows impellers are used. Circulation flow rate, Q_{C}, is then defined as:

$$Q_{\mathrm{C}} = \frac{V}{t_{\mathrm{C}}} \tag{8}$$

This determination of the circulation time or the circulation flow rate needs time-dependent information.

The circulation flow rate is also defined for an impeller [16] as the sum of the impeller flow rate, Q_{Fl}, and the flow rate generated by momentum transfer, Q_{e}:

$$Q_{\mathrm{C}} = Q_{\mathrm{Fl}} + Q_{\mathrm{e}} \tag{9}$$

For a single impeller system, assuming an angular symmetry, Jaworski et al. [8] define the circulation flow rate as:

$$Q_{\mathrm{C}} = \max_r\{|Q_r|\} = \max_z\{|Q_z|\} \tag{10}$$

where:

$$Q_z = 2\pi \int_{r_1}^{r_2} r(\overline{v_z})_z \,\mathrm{d}r \tag{11}$$

$$Q_r = 2\pi r \int_{z_1}^{z_2} (\overline{v_r})_r \,\mathrm{d}z \tag{12}$$

Extending this concept, Aubin [18] specifies that the circulation flow rate could be the flow rate generated in any circulation loops:

$$Q_z = \int_r^R 2\pi r \,|v_z| \,\mathrm{d}r \tag{13}$$

where r is the radial coordinate of the centre of the loop and R is the radius of the tank. This approach allows to consider the case where two circulation loops are produced. The overall flow rate is the sum of the circulation flow rates of the two loops (Fig. 2). Extending this concept to more than two loops should be done very carefully, particularly, this concept is difficult to extend for multiple impellers systems for two reasons:

- this measure confuses the local and the overall circulation;
- the local circulation is not very significant for these systems.

Moreover, in systems where axial symmetry is far from effective, the circulation loop cannot be used and the circulation number is less representative.

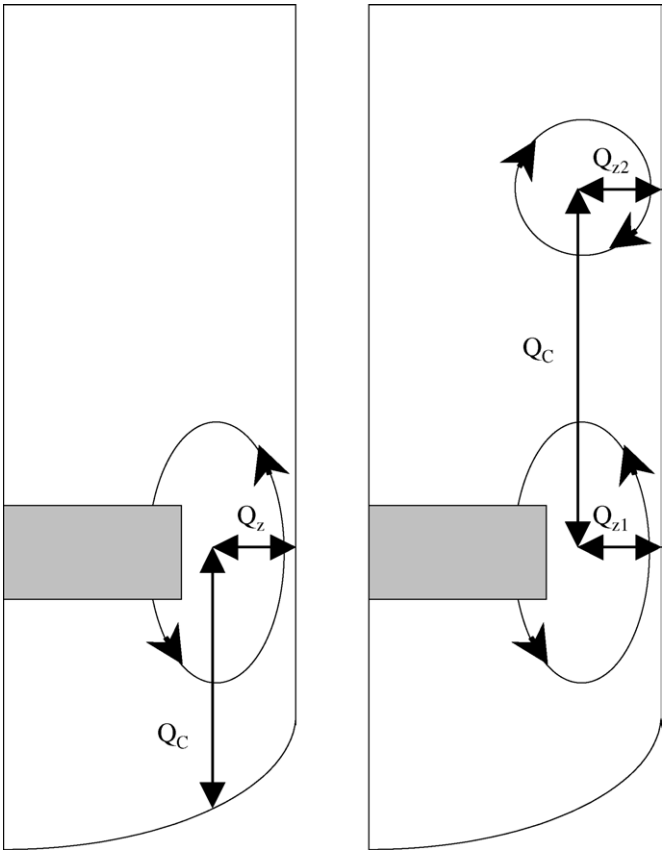

Fig. 2. Circulation flow rate for one and two loops. For one loop, $Q_{\mathrm{C}} = Q_z$; for two loops, $Q_{\mathrm{C}} = Q_{z1} + Q_{z2}$.

Circulation is represented dimensionless, using circulation number, N_C, defined as:

$$N_C = \frac{Q_C}{ND^3} \tag{14}$$

2.2.3. Axial flow number and average axial circulation time

Since the previous numbers do not characterize well enough the loops connection, an axial flow number is defined [3].

The axial flow rate, Q_{ax}, at different heights in the vessel is evaluated by the surface integration of either the positive, v_z^+, or negative, v_z^-, component of the axial velocity at particular horizontal plane:

$$Q_{ax}(z) = \int_A v_z^+ \, dA = \int_A v_z^- \, dA \tag{15}$$

where A is the radial section of the tank.

The average axial flow rate, Q_{Aax}, for the entire vessel is defined as:

$$Q_{Aax} = \frac{\int_0^H Q_{ax}(z) \, dz}{\int_0^H dz} \tag{16}$$

Both the axial flow rate and the average axial flow rate can be normalised by ND^3 to give the dimensionless axial flow number, $N_{Q_{ax}}$, and the dimensionless average axial flow number, $N_{Q_{Aax}}$, respectively:

$$N_{Q_{ax}}(z) = \frac{Q_{ax}(z)}{ND^3} \tag{17}$$

$$N_{Q_{Aax}} = \frac{Q_{Aax}}{ND^3} \tag{18}$$

The following relation defines the average axial circulation time, t_{ax}:

$$t_{ax} = \frac{V}{Q_{Aax}} \tag{19}$$

2.3. Volume-weighted average velocity and agitation index

The volume-averaged velocity is used for comparing the movement intensity in different configuration or with different operating conditions of a tank. For this purpose, it is postulated [19] that each velocity v_{ijk} corresponds to a volume of liquid vol_{ijk}, which is related to the vessel dimensions and the grid point coordinates, i, j, k. The volumes corresponding to the whole grid are summed, so that a volume-averaged velocity, $\hat{V}$, is obtained:

$$\hat{V} = \frac{\sum_i \sum_j \sum_k v_{ijk} \mathrm{vol}_{ijk}}{\sum_i \sum_j \sum_k \mathrm{vol}_{ijk}} \tag{20}$$

where the denominator corresponds to the liquid volume.

Dividing this volume-averaged velocity by the impeller tip velocity, V_{tip}, yields the agitation index I_g [19]:

$$I_g = 100 \frac{\hat{V}}{V_{tip}} \tag{21}$$

which may be considered as representing the global mean velocity expressed as a percentage of the tip velocity. The agitator index is a measure of the effectiveness of a particular geometry in inducing a flow in the whole bulk.

2.4. Velocity fields and streamlines

Velocity fields and streamlines are sometimes the main used method to analyse the flow [15].

Tangential velocity components are most often so high compared to axial and radial components that the mixing in that direction is not a limitation. Therefore, in order to understand the flow, results, especially velocity vectors are often presented on two-dimensional maps with colour range or with vectors of length proportional to the norm of the velocity vectors.

Streamlines are three-dimensional curves tangent to velocity vectors.

Since three-dimensional curves are not easy to understand. Curves tangent to two-dimensional vector projections are often used, especially to show circulation loops. However, those representations assume an angular symmetry and may be very confusing as shown in the instructive example presented in Fig. 3. Four planes are presented following particles tangential velocity. The curves tangent to two-dimensional vector projections on the four planes may be identified as belonging to interrelated loops. However, the particles stay in the upper, middle or lower part of the tank.

2.5. Particles tracking

The goal of the particle tracking is to highlight the dead zones, by-pass or partial confined mixing zones (as invariant tori, confirmed by KAM—Kolmogorov–Arnold–Moser theorem quoted by Ottino [21]). For this, a particle is injected in the tank at different positions in the bulk. Particle tracking is carried out using the discrete phase model. It consists in following the trajectory of pieces of fluids considered as fluid particles. This means that the trajectories are calculated using inert and spherical particles with a small diameter (for example, 10 μm) and a density close to the fluid density, and a motion written in a Lagrangian reference frame:

$$\frac{ds}{dt} = v_P \tag{22}$$

where s is the particle position and v_P is the particle velocity. The procedure is uncoupled, which means that the particle traces are resolved from the previously determined velocity fields.

For a stirred vessel, with rotating reference frame or with moving reference frame modelling, the particles tracking is not a real Lagrangian analysis since a particle trajectory is calculated with a fixed impeller. In the first case, there is just a reference difference. The trajectory of theses particles gives a three-dimensional idea of the fluid motion and may highlight the dead zones or by-pass. For multiple impellers systems, it may show if the circulation is global or not. For non-axial symmetric flows and more particularly laminar flows, it can reveal the oscillation phenomenon shown on Fig. 3.

The different criteria defined in this section are used in Sections 4 and 5 to understand industrial examples.

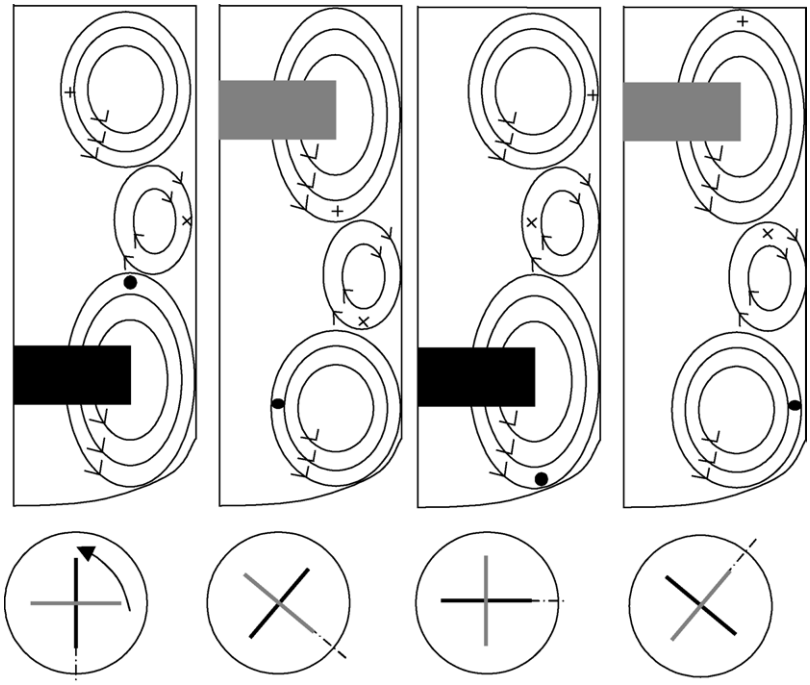

Fig. 3. Instructive example of streamlines presenting false interconnected loops. Arrows indicate streamlines. (●, ×, +) Particles. Each figure on the lower part presents the position of the impellers and the position of the plane represented on the corresponding figure on the upper part.

3. Modelling and numerical aspects

Since the simulation of the process in its whole complexity would be very unrealistic, in order to simplify the hydrodynamic, the simulation considers single-phase flows without heat transfer. Time constants relative to the flow or to the heat transfer have very different order of magnitude, so the simulation of the two coupled phenomena would be useless. The viscosity is set to the values in which the mixing is the most critical.

Fluent® 6.0.20 is used in the simulations carried out to solve the momentum and continuity equations for the laminar fluid flow. Since *Re* is around 100, the flow regime is transient close to the laminar regime. As it has been done by Kelly and Gigas [4], the macro-instabilities that may happen at this transient flow regime close to laminar regime are neglected and the flow is modelled using laminar equations. A no-slip boundary condition is imposed on all walls. The free liquid surface is modelled with no vortex, a zero-flux and zero-stress conditions. The absence of baffles enables to use the usual "Rotating Reference Frame" (RRF) approach to model the impellers motion. This technique models the motion of the tank in the impellers reference frame. All terms of the equations are discretised using the second-order upwind differencing scheme and the equations are solved using the SIMPLE algorithm.

Simulations are typically considered converged when the velocity residuals fall below 10^{-7}. Further checks for convergence are made by verifying that the computed power number remained constant.

The commercial mesh generator Gambit® 2.0.4 is used to create an unstructured tetrahedral mesh due to the complex geometry of the impellers. Periodic symmetry of the geometry enables to reduce the computational domain and thus a valuable reduction in computational expenses. The mean cell edge length is about 0.06 m. A preliminary grid convergence study has been carried out in order to verify that the solution was grid independent for this cell edge length. The number of computational cells used is about 160 000 cells for the first example and about 505 000 for the second one.

Since used equations do not contain any modelling assumption, there are few reasons for the numerical results to be unlike experimental one. Some differences may come:

- from the quality and granularity of the mesh and from the discretisation scheme in relation to the physical phenomena;
- from the transient-laminar assumption mention earlier;
- from the top surface modelling.

All these assumption have been previously validated by Letellier et al. [3].

4. Example 1: industrial tank containing double-flow impellers

4.1. Description of the system

The tank is equipped with three impellers (Fig. 4a and Table 1): two double flow impellers and a pitched blade turbine (PBT) in the bottom. The double flow impellers are SGDF from Milton Roy Mixing®. They have a complex geometry: the down-pumping blade, which is closer to the shaft, is an irregular hexagon on a curve surface, the up-pumping blade, which is closer to the wall looks like a shovel of a snow-plough. They may be equipped or not with a vertical blade. The PBT is made with four blades at 45°. The periodic symmetry of the

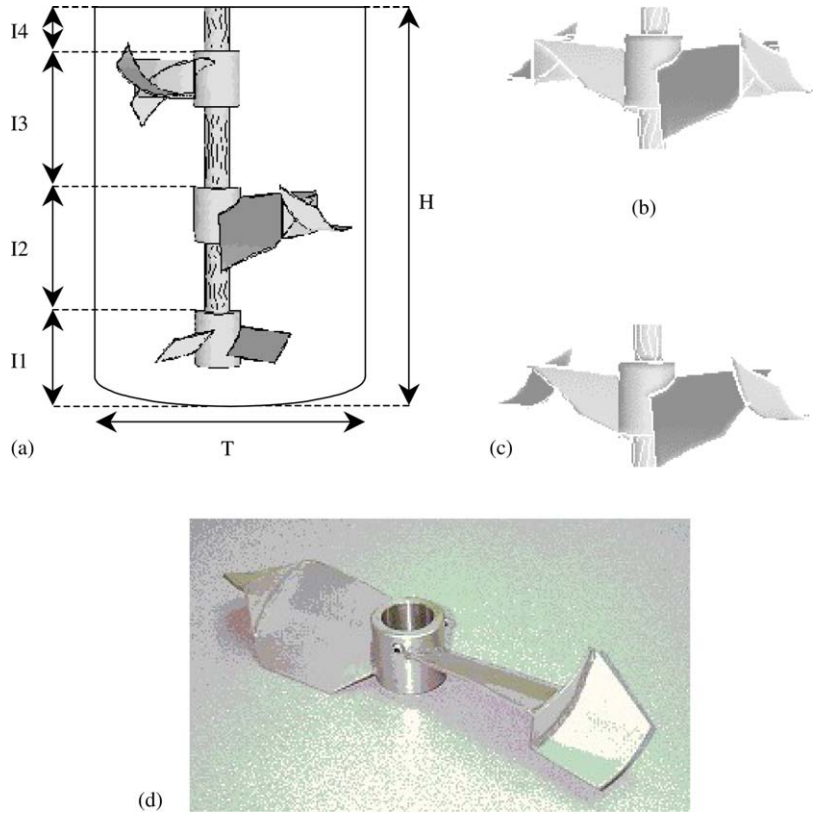

Fig. 4. Half tank (a); impellers with the vertical blade (b); impellers without the vertical blade (c); picture of the impellers with vertical blade (d).

geometry enables to model only one half of the tank. The study presented here is about the influence of the vertical blade – a plate, part of the double-flow impeller, set vertically in-between the down-pumping blade and the up-pumping blade to enforce the structure – for the two double-flow impellers. Fig. 4b shows a double-flow impeller with the vertical blade and Fig. 4c a double-flow impeller without the vertical blade. The objective of the work is to verify that this vertical blade has no bad influence on the circulation. For this purpose, a simulation is done with the blade and another one without.

This kind of stirrer and more generally double flux stirrer are well adapted to both laminar and transient flows [3]. Therefore, they give good performance in the case of indirect emulsification (phase inversion process) of highly viscous resins like epoxy or polyester (alkyd resins), for which the viscosity and the rheology of the media are varying drastically all along the emulsification process [22]. Modelling has been approached by considering the bulk pseudohomogeneous (i.e. constant density and viscosity) at the most critical point of the process.

The resin has not a huge density ($\rho = 1100\ \mathrm{kg/m^3}$), is highly viscous but remains Newtonian ($\mu = 30$ Pa s). The rotating speed gives a rather low Reynolds number ($Re = 95.3$).

4.2. Results and analysis

Powers consumption, presented in Table 2, shows that the use of the vertical blade has no significant effect.

Local axial flow numbers are presented in Fig. 5. Average axial flow number, $N_{Q\mathrm{Aax}}$, and axial circulation time, t_{ax} are presented in Table 3. Considering the uncertainty of numerical simulations, it is difficult to have a definite conclusion.

Table 1
System dimensions for the first example

Vessel diameter, T (m)	2.4
Liquid height, H (m)	3.4
Liquid volume, V (m^3)	14.6
Double-flow impeller diameter, D_{DF} (m)	2.28
Pitched blade turbine diameter, D_{PBT} (m)	1.44
Distance bottom – PBT, I_1 (m)	0.4
Distance PBT – DF_1, I_2 (m)	$D/2 = 1.14$
Distance DF_1 – DF_2, I_3 (m)	1.0
Distance DF_2 – free liquid surface, I_4 (m)	0.8
Blades thickness (m)	0.012

Table 2
Power consumption calculated by the torque method and the viscous dissipation method for the first example

Simulation	With vertical blade	Without vertical blade
Torque on impellers		
P (W)	18833	18960
P_0	2.22	2.24
P_0Re	212	213
Viscous dissipation		
P (W)	19705	20111
P_0	2.33	2.37
P_0Re	222	226

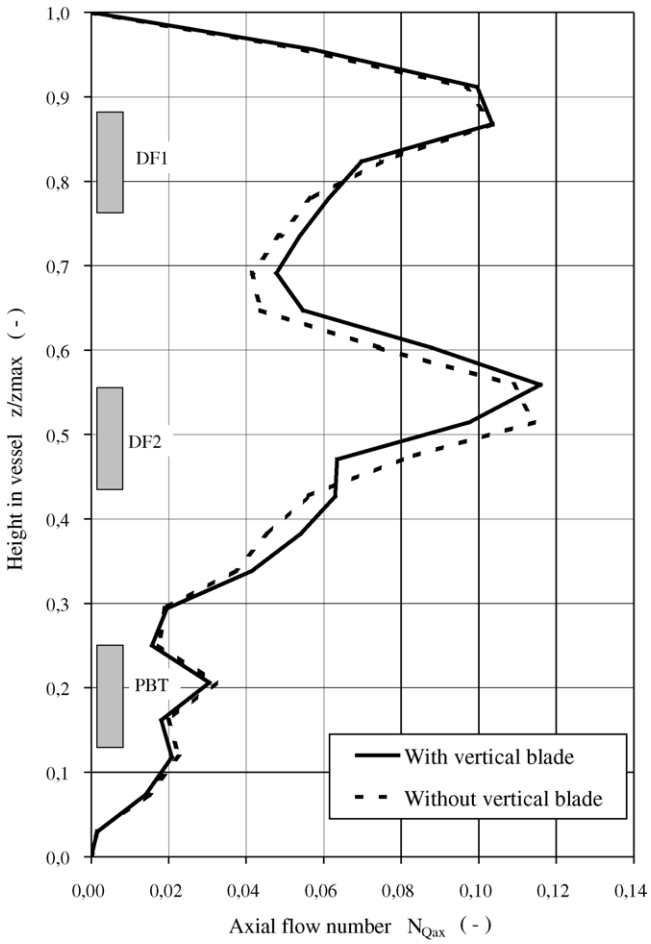

Fig. 5. Axial flow number for different height in the vessel for the simulation with and without vertical blades. The locations of the impellers, two double flow impellers (DF_1 and DF_2) and a pitch blade turbine (PBT) are indicated by the rectangles.

However, the trend of all parameters is similar; the slight variation in axial circulation time and the higher flow under the double flow impellers shown by the local axial flow number show that the use of the vertical blade slightly increases the overall circulation. This slight improvement of the flow patterns, especially the better circulation between each stage of impeller may be explain by the effect of the vertical blade on the flow which would be similar to a guide tube one.

Table 3
Axial circulation characteristics for the first example

Simulation	With vertical blade	Without vertical blade
Average axial flow number, $N_{Q_{Aax}}$	0.052	0.051
Axial circulation time, t_{ax} (s)	46.9	48.0

Fig. 6, showing the traces of particles axially distributed, each one having its own colour, confirms this assumption. Fig. 6a and b shows a poor circulation between the first propeller and the second double flux propeller. Fig. 6a shows a better mixing of the colour between the second double flux propeller and the PBT, indicating a better axial circulation.

4.3. Conclusions

Axial flow rates give relevant information for the comparison of impellers shape: the vertical blade induces a slightly better distribution of the axial flow rates, which means a small increase of the overall circulation. The power calculation shows that the vertical blade does not make the power consumption higher. Therefore, the rather good influence of the vertical blade on the circulation and on energy consumption shows that this vertical blade should be retained.

5. Example 2: tank containing impellers and a coil heat exchanger

5.1. Description of the system

The tank contains two axial agitators and a helical coil heat exchanger. Influences of the viscosity and of the heat exchanger diameter on the flow are studied.

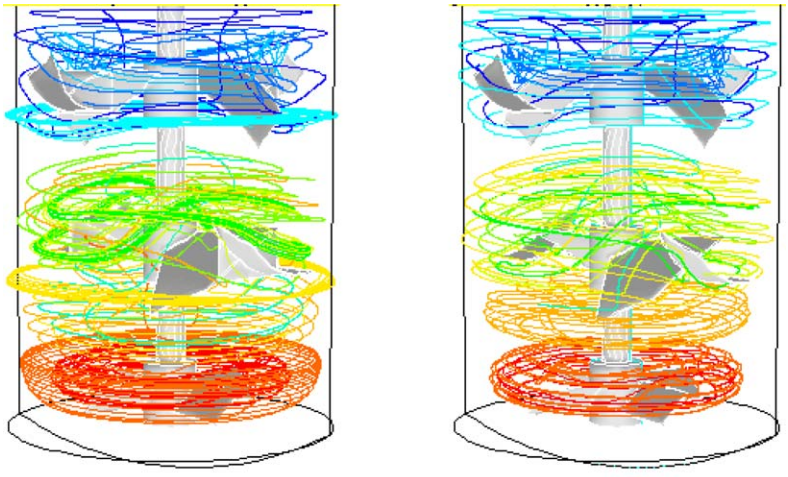

Fig. 6. Particles traces shown by particles ID: (a) with vertical blades; (b) without vertical blade.

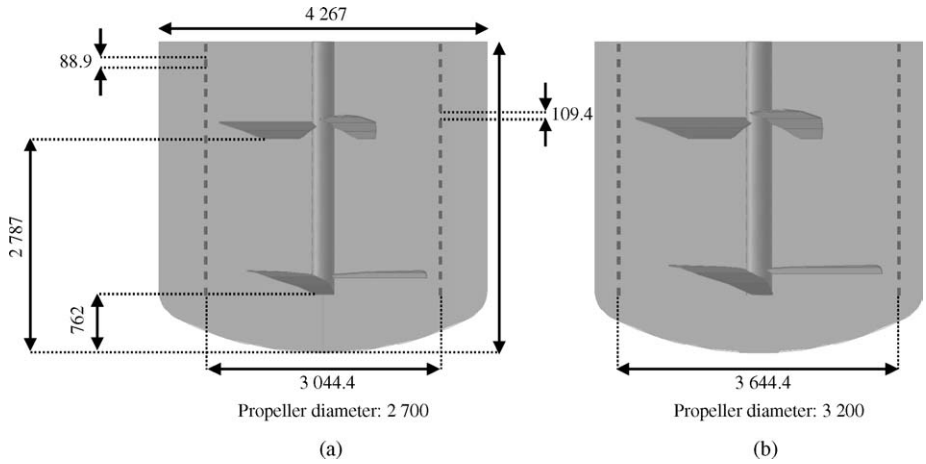

Fig. 7. Simulated geometry (dimensions in mm): (a) $S = 0.7T$; (b) $S = 0.83T$.

Table 4
Operating conditions for the second example

Coil diameter, S (m)		$3044.4 - 0.7T$		$3644.4 - 0.83T$
Rotational speed, N (min^{-1})		27		23
Impeller diameter, D (m)		2.7		3.2
Impeller tip velocity, V_{tip} ($m\,s^{-1}$)		3.8		
Liquid rheology		Newtonian		
Liquid viscosity, μ (Pa s)	25	40	60	25
Liquid density, ρ ($kg\,m^{-3}$)		1100		
Reynolds number, Re	144	90	60	173

The liquid height in the tank chosen for the simulation corresponds to one of the process key steps. Only one coil layer is present with a diameter S divided by the reactor diameter T equal to 0.7 (Fig. 7a) or 0.83 (Fig. 7b). The mixing system is composed by two Mixel^{TM} TTP three-blade propellers [20] of diameter D depending of the coil diameter, $D/S = 0.9$. The propellers work on the down-pumping mode and are shifted of 60° one compared to another. The lower plane of the lower propeller corresponds to the lowest row of the coil. The second propeller is at a height of $0.75D$. Operating conditions are listed on Table 4. The propeller tip velocity is maintained constant when the propeller diameter is changed.

The heat exchanger is modelled by a series of rings having zero-thickness and a height equivalent to the heat exchanger tube diameter. Therefore, the simplified geometry of the heat exchanger is not modelled as a spiral. Periodic symmetry of the geometry enables to model only one-third of the vessel.

5.2. Results

5.2.1. Power consumption

The power consumption for each simulation is calculated via the volume integration of the viscous dissipation (Eq. (1)) and via the torque method (Eq. (3)). The difference between the two methods increases with the viscosity. The maximum difference is about 6% (Table 5). In laminar regime, power numbers should increase proportionally to the viscosity. As the P_0Re values (Table 5) are not constant, the flow regime is transient. Table 6 shows the breakdown of the power consumption between the different agitators. For a fixed value of the viscosity, the power used by the lower Mixel^{TM} TTP propeller is the same as the power used by the upper one. The effect of the increase of the

Table 5
Power consumption calculated by the torque method and the viscous dissipation method for the second example

S	μ (Pa s)	Re	Torque on impellers		Viscous dissipation	
			P_0	P_0Re	P_0	P_0Re
	25	144	1.23	178	1.27	183
$0.7T$	40	090	1.75	142	1.65	149
	60	060	1.99	120	2.11	127
$0.83T$	25	173	1.16	200	1.19	206

Table 6
Breakdown of power consumption for the second example

	P (W)			
	$S = 0.7T$			$S = 0.83T$
	$\mu = 25$ Pa s	$\mu = 40$ Pa s	$\mu = 60$ Pa s	$\mu = 25$ Pa s
Lower propeller	08 843	11 267	14 139	12 100
Upper propeller	08 827	11 220	14 245	11 950
Shaft	00 090	00 144	00 212	00 063
Total	17 760	22 631	28 596	24 113

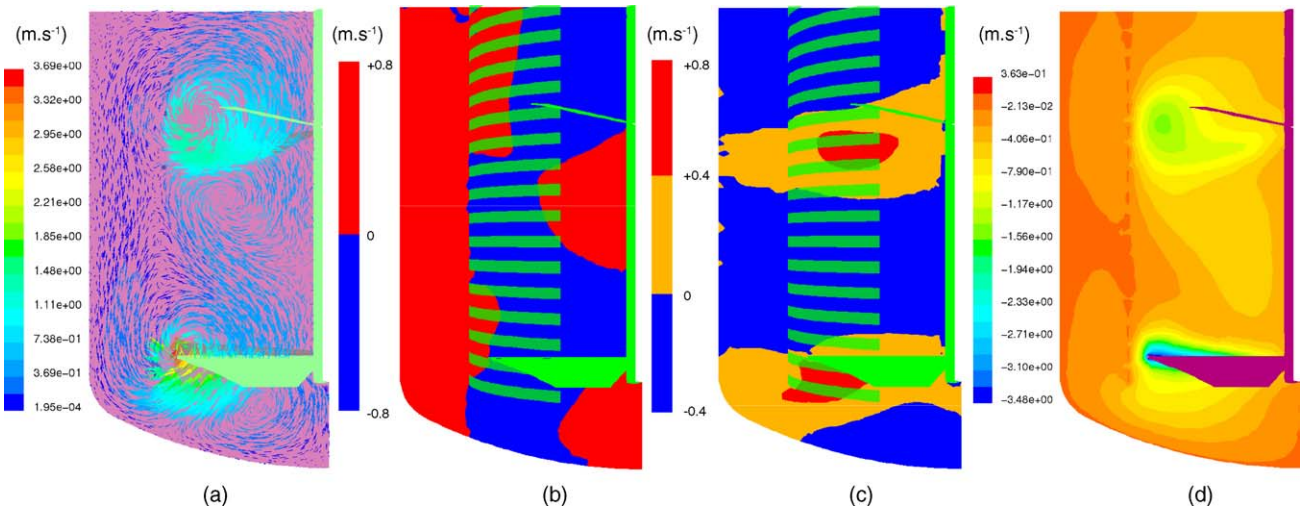

Fig. 8. Flow field for the small diameter coil ($S = 0.7T$) for a viscosity of 25 Pa s: (a) mean velocity field; (b) axial velocity contour; (c) radial velocity contour; (d) tangential velocity contour.

coil diameter on power consumption cannot be evaluated since the propeller diameter increases as well.

5.2.2. *Mean velocity field*

Flow fields are visualised on a plane passing through the middle of one blade of the lower propeller and between two blades of the upper propeller. The flow is identical for other tangential positions. The region between the heat exchanger and the wall is called "external zone" and the region inside the heat exchanger with the two propellers is called "internal zone".

5.2.2.1. Influence of the viscosity. Five circulation loops are visible on the mean flow field (Fig. 8a). Two circulation loops are visible at agitators tip (self-feeding). The discharge flow of the propeller is relatively oblique, which is normal as an axial impeller becomes a radial impeller at low *Re*. One little circulation loop is situated below each impeller. The axial movement in the external zone of the tank is well present. However, the intensity in the tank bottom is stronger due to the impact of discharge flow of the lower propeller against the dished bottom. One part of the discharge flow of the upper agitator goes down and is picked up by the lower agitator bypassing the circulation loop situated below the upper agitator. Main velocity fields are very similar whatever the viscosity used. That is the reason why the velocity field is shown for only one viscosity. However, when the viscosity increases, the discharge flow becomes more radial, the volume of the circulation loops below the propeller increases and the axial movement in the external zone decreases.

The axial velocity contour (Fig. 8b), rather identical for the three viscosities, shows that the flow is down-coming in the internal zone and rising in the external zone.

Qualitatively, the radial velocity contour (Fig. 8c) does not change with the viscosity. Differences only come from the size diminution of strong radial velocity core at the tip of each impeller. The radial flux of the upper propeller also decreases with an increase of the viscosity.

The only difference visible on the tangential velocity contour (Fig. 8d) is its intensity, which decreases in the external zone with the increase of the viscosity. The tangential velocity spreads in the external zone by spaces between coil tubes. An entrainment effect is also seen, because the tangential velocity core is bigger than the impeller height.

To sum up, the increase in the viscosity from 25 to 60 Pa s changes the intensity of the velocity vector components, but the general scheme of the flow field remains the same. The decrease of the velocity vectors components with the increase in the viscosity is due to an increase of the viscous forces. In this case, up to 60 Pa s, the flow field is enough efficient to allow a good homogenization of the products and a good circulation in the tank.

5.2.2.2. Influence of the coil diameter. The increase in the coil diameter induces a volume increase of the circulation loop situated below the upper propeller. This circulation loop takes all the space between the shaft and the coil. This can be seen either on the mean velocity field (Fig. 9a) and the axial velocity contour (Fig. 9b). Apparently, no connection exists between the flow induced by the two propellers in the internal zone. The flow in the external zone is weaker, above all in the zone between the two agitators.

5.2.3. *Global criteria for the flow analysis in the external zone*

It is useful to have global criteria to characterize the flow in the external zone. Fig. 10 shows the evolution of the volume averaged velocity and the agitation index in the external zone with the viscosity and the coil diameter. These two criteria decrease when the viscosity and the coil diameter increase. This is consistent since increasing the viscosity induces higher viscous forces. The volume averaged velocity and the agitation index in the external zone also decrease with an increase of the coil diameter from $0.7T$ to $0.83T$. This is not favourable of the homogenization and cooling processes, which need a great axial

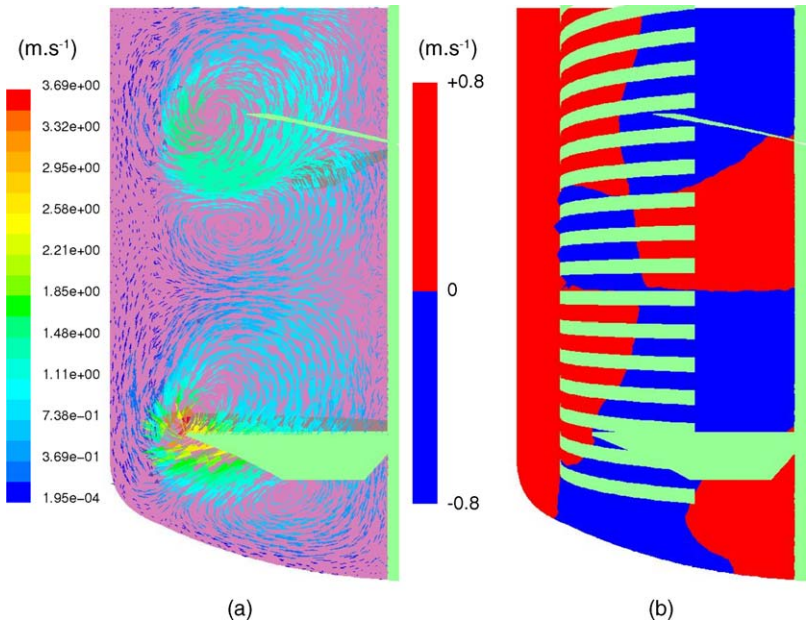

Fig. 9. Flow field for the large diameter coil ($S = 0.83T$) for a viscosity of 25 Pa s: (a) mean velocity field; (b) axial velocity contour.

circulation in the external zone. The volume averaged velocity and the agitation index criterion allow well to characterize the flow intensity in the external zone of the tank.

5.2.4. *Axial flow number*

Axial flow number profiles along the tank are presented on Fig. 11. These profiles are in accordance with what was expected and present a peak for each propeller. These peaks are identical and situated a little above the middle plane of the propeller. Their intensity decreases with an increase in the viscosity. When the coil diameter increases, a high minimum is observed between the two propellers. This confirms the decrease in the connection between the two propellers.

Table 7 shows a decrease of the average axial flow number with an increase in viscosity in accordance with what was expected. This goes together with an increase in the average axial circulation time. The average axial flow number increases with the coil diameter, whereas the average axial circulation time decreases. This comes from the increase in the propeller

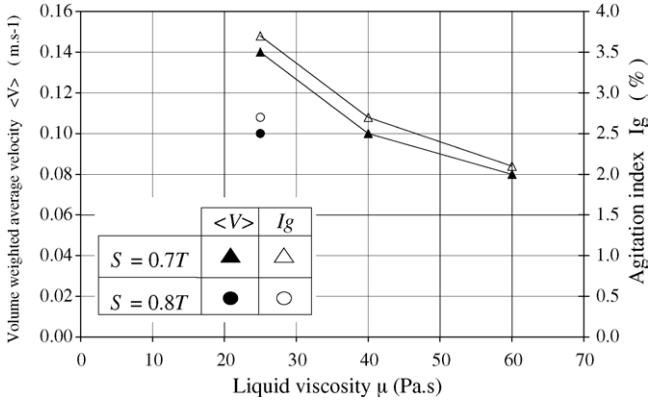

Fig. 10. Influence of the viscosity and the coil diameter on the volume weighted average velocity and the agitation index in the external zone.

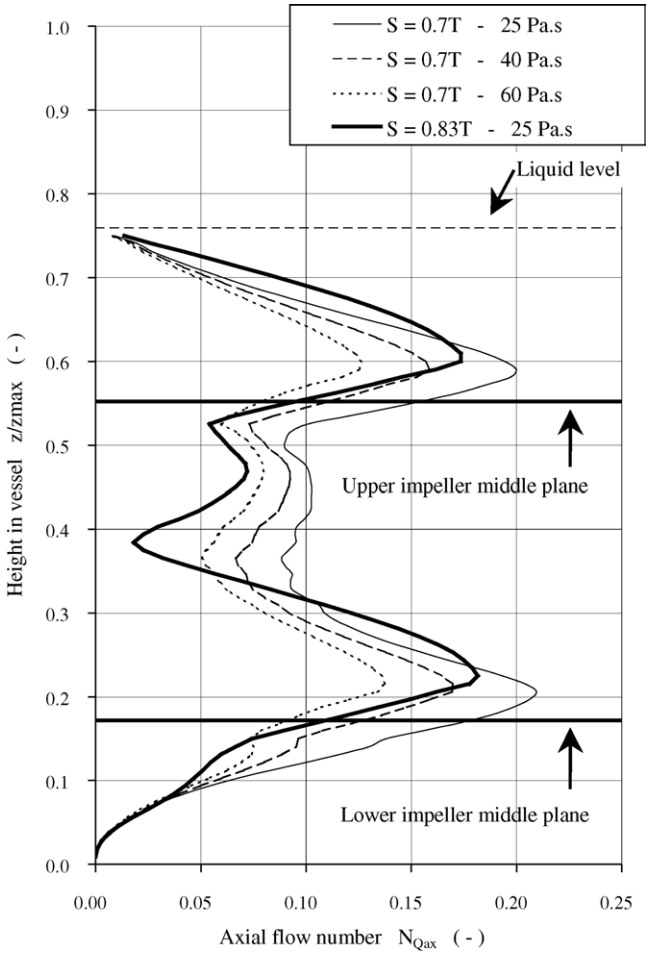

Fig. 11. Axial flow number for different height in the vessel.

Table 7
Axial circulation characteristics for the second example

S	μ (Pa s)	$N_{Q_{Aax}}$	t_{ax} (s)	Nt_{ax}
	25	0.109	55.4	24.9
0.7T	40	0.089	67.8	30.5
	60	0.073	82.8	37.3
0.83T	25	0.088	48.5	18.6

diameter due to the use of a larger coil diameter. Nt_{ax} also decreases.

5.2.5. Particle tracking

Initially, the velocity of the particle or of the group of particles is set to $v_x = -2\ \mathrm{m\,s^{-1}}$ which represents a radial velocity towards the shaft.

5.2.5.1. Influence of the viscosity. Many axial and radial injection positions for the three viscosities have been tested. The figures are presented for only one viscosity and a summary of the whole results is presented in Table 8. These results should be considered with particular attention since the final time cannot be always the same. However, the influences written in Table 8 are confirmed by several tests. In a general way, little circulation is present between the internal and the external zone and a dead zone is present under the lower impeller.

The tank bottom is a sensitive region for the injection position (Fig. 12). When the viscosity increases, the particle has more chance to be trapped and to stay in the circulation loop situated below the lower propeller. If an injection has to be placed in the tank bottom, it should be situated between the wall and the coil to avoid this problem.

As presented in Table 8:

- If the particle is injected at the upper plane of the lower propeller, trajectories can be classified in two categories. In the first category of trajectories (particle released at $r = 1.6$ m), the particle passes near the coil and remains around the lower propeller and never goes around the upper propeller. In the second category of trajectories (particle released at $r = 2.0$ m), the particle goes in the entire tank and so crosses the volume swept by each impeller. If the particle is released at $r = 1.8$ m (i.e. at a radial position between the two above one), the particle will pass alternatively from the trajectory of the first category to the trajectory of the second one.
- If the particle is injected near the liquid surface, the observed effects are difficult to explain. This can be attributed to the description of the liquid surface as a plane surface. Since a vortex certainly exists, the velocity field in this region is not correctly predicted.
- The influence of the viscosity on particle trajectory is less important than the influence of the injection position. However, the influence of viscosity is key in some sensitive cases, where the circulation of the newly input material could be correct with the lower viscosity and not correct with the higher viscosity (for example, for $z = 0.5$ m and $r = 1.2$ m).

5.2.5.2. Influence of the coil diameter. For the bigger coil diameter, $S = 0.83T$, when the particle is injected below the lower propeller near the shaft or near the coil, it goes out from this zone and circulates in the rest of the tank. But, if the particle is released between these two positions, it circulates only in the lower half of the vessel with some difficulty.

For an injection at the upper plane of the lower propeller between the coil and the wall, the particle circulates without any problems in the whole tank. The connection between the two propellers exists but it is a weak one. The self-feeding loops of each propeller predominate on the flow.

If the particle is released near the liquid surface between the coil and the wall, there is only one position for which the particle goes in the whole vessel. For the two other ones, the par-

Table 8
Abstract of particles tracking results for the second example

r (m)		Volume swept by the particle injected			
$S = 0.7T$	$S = 0.83T$	$S = 0.7T$			$S = 0.83T$
		$\mu = 25$ Pa s	$\mu = 40$ Pa s	$\mu = 60$ Pa s	$\mu = 25$ Pa s
Liquid surface, $z = 4.0$					
1.6	1.9	Whole tank	Whole tank	Whole tank	Blocked below the upper propeller
1.8	2.0	Whole tank	Whole tank	Whole tank	Whole tank
2.0	2.1	Whole tank	Blocked below the lower propeller	Whole tank	Blocked around the lower propeller
Upper plane of the lower propeller, $z = 1.0$					
1.6	1.9	Lower part of the tank	Lower part of the tank	Lower part of the tank	Whole tank
1.8	2.0	Whole tank	Whole tank	Whole tank	Half tank, then blocked below the lower propeller
2.0	2.1	Whole tank	Whole tank	Whole tank	Upper part of the tank
Below the lower propeller, $z = 0.5$					
	0.6	Blocked below the lower propeller	Blocked below the lower propeller	Blocked below the lower propeller	Blocked below the lower propeller
	1.2	Whole tank	Blocked below the lower propeller before circulating in the whole tank	Blocked below the lower propeller	Lower part of the tank
	1.8	Whole tank	Whole tank	Whole tank	Whole tank

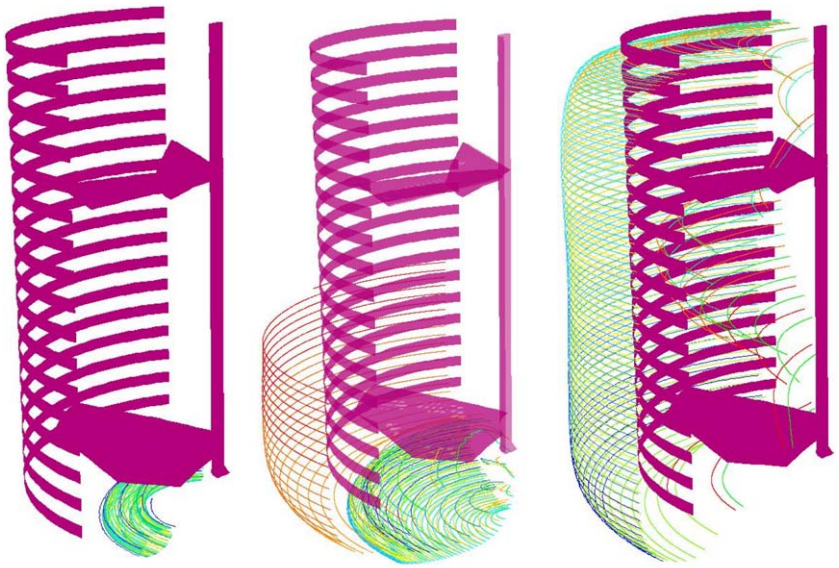

Fig. 12. Effect of radial release position for a viscosity of 40 Pa s: single particle traces colored by residence time.

ticles are blocked below the upper propeller or around the lower propeller.

In the single case of particle injection just below the lower impeller, this particle tracking shows surprisingly better circulation for a larger coil diameter. For the other injections (upper plane of the lower propeller and liquid surface) the circulation is more difficult in the case of coil larger than 0.7*T*.

5.3. Conclusions

A flow in the whole tank has been shown: the liquid is down-coming inside the coil and rising between the coil and the wall. A radial movement is also visible: the fluid is pushed to the wall through the coil at the level of the impeller and comes back to the shaft through the coil between the impellers. The mean velocity in the external zone is about 4% of the impeller tip velocity. Recirculation loops are visible below each propeller.

The particle tracking has shown that the two propellers work together. The particles rise in the external zone and are down-coming in the internal zone. They pass through the two propellers. They avoid the circulation loops placed below the impeller, showing possible dead zones. Then, the lower propeller pushes the particles under the coil in the external zone. The injections points to be avoided are these placed below the lower plane of the lower impeller and these near the coil.

The simulations of two different coil diameters, 0.7*T* and 0.83*T*, show a modification of the flow. The biggest difference comes from the upper propeller circulation loop, which takes place from the shaft to the coil. But, this is not so clear, depending in the tangential position of the visualisation plane. However, the particle tracking has partially confirmed this fact. The smaller coil diameter offers most of the time a better circulation except for particle injection just below the lower propeller.

6. General conclusions

Since it is not always possible to simulate industrial cases in their whole complexity, CFD simulations may give interesting information if results analysis is well performed. In this article, results analysis tools for laminar or transient-laminar, single-phase flow in a multi-stage tank are presented and applied to industrial cases. The power or power numbers give information about the functioning cost. The axial flow numbers show an influence of the configuration in the connection between the propellers. Despite the fact that the circulation is more important above the impellers, the axial flow numbers show, in the first case, that the vertical blade used to enforce the structure of the impeller has a fairly good effect on the axial circulation. In the second case, the increase of viscosity makes as expected the circulation lower and the increase of the impeller diameter unexpectedly makes the circulation decreasing. The velocity profiles give relevant information to check the consistency of the flow. The particles tracking is necessary to understand the three-dimensional feature of the flow, especially to point out that the two propellers do not work together in the first example (Section 4) and do work together in the second example (Section 5).

Appendix A. Nomenclature

A	axial section of the tank (m^2)
C	torque (N m)
D, D_{DF}, D_{PBT}	impeller diameter (m)
Fl	flow number ($=Q_{Fl}/ND^3$)
H	liquid height in the tank (m)
I_1	distance tank bottom – pitched blade turbine (m)
I_2	distance pitched blade turbine – DF1 impeller (m)

I_3 distance DF1 impeller – DF2 impeller (m)
I_4 distance DF2 impeller – free liquid surface (m)
I_g agitation index (%)
k turbulent kinetic energy ($m^2\,s^{-2}$)
N impeller rotation speed (s^{-1})
N_C circulation number ($=Q_C/ND^3$)
$N_{Q_{Aax}}$ average axial flow number ($=Q_{Aax}/ND^3$)
$N_{Q_{ax}}(z)$ axial flow number ($=Q_{ax}(z)/ND^3$)
P agitation power consumption (W)
P_0 power number ($=P/\rho N^3D^5$)
Q_{Aax} average axial flow rate ($m^3\,s^{-1}$)
$Q_{ax}(z)$ axial flow rate ($m^3\,s^{-1}$)
Q_C circulation flow rate ($m^3\,s^{-1}$)
Q_e flow rate generated by momentum transfer ($m^3\,s^{-1}$)
Q_{Fl} pumping flow rate ($m^3\,s^{-1}$)
Q_z, Q_{z1}, Q_{z2} loop circulation flow rate ($m^3\,s^{-1}$)
r radial coordinate (m)
R tank radius (m)
Re Reynolds number ($=\rho ND^2/\mu$)
s particle position (m)
S heat exchanger coil diameter (m)
t time (s)
t_{ax} average axial circulation time (s)
t_C circulation time (s)
t_s end time for particle tracking (s)
T tank diameter (m)
v velocity ($m\,s^{-1}$)
v_P particle velocity ($m\,s^{-1}$)
v_x, v_y, v_z cartesian velocity component ($m\,s^{-1}$)
V liquid volume (m^3)
$\hat{V}$ or $\langle V\rangle$ volume-weighted average velocity ($m\,s^{-1}$)
V_{tip} impeller tip velocity ($m\,s^{-1}$)
x, y, z cartesian coordinates (m)
z_{max} maximal axial position (m)

Greek letters
Φ_V viscous dissipation (s^{-2})
ε energy dissipation rate ($m^2\,s^{-3}$)
μ fluid viscosity (Pa s)
η apparent fluid viscosity (Pa s)
ρ fluid density ($kg\,m^{-3}$)

References

[1] M. Sommerfeld, S. Decker, State of the art and future trends in CFD simulation of stirred vessel hydrodynamics, Chem. Eng. Technol. 27 (2004) 215–224.
[2] F. Thibault, P. Tanguy, Power drawn analysis of a coaxial mixer with Newtonian and non-Newtonian fluids in the laminar regime, Chem. Eng. Sci. 57 (2002) 3861–3872.
[3] B. Letellier, C. Xuereb, P. Swaels, P. Hobbes, J. Bertrand, Scale-up in laminar and transient regimes of multi-stage stirrer, a CFD approach, Chem. Eng. Sci. 57 (2002) 4617–4632.
[4] W. Kelly, B. Gigas, Using CFD to predict the behaviour of power law fluids near axial-flow impellers operating in the transitional flow regime, Chem. Eng. Sci. 58 (2003) 2141–2152.
[5] B. Zakrzewska, Z. Jaworski, CFD modelling of turbulent jacket heat transfer in a Rushton turbine stirred vessel, Chem. Eng. Technol. 27 (2004) 237–242.
[6] A. Brucato, M. Ciofalo, F. Grisafi, R. Tocco, On the simulation of stirred tank reactors via computational fluid dynamics, Chem. Eng. Sci. 55 (2000) 291–302.
[7] J. Derksen, Simulation of solid particle dispersion in agitated tanks, in: Proceedings of 11th Conference on Mixing, Bamberg, Germany, VDI-GVC, 2003, pp. 121–128.
[8] Z. Jaworski, A. Nienow, K. Dyster, An LDA study of turbulent flow field in a baffled vessel agitated by an axial down pumping hydrofoil impeller, Can. J. Chem. Eng. 74 (1995) 3–15.
[9] P. Gogate, A. Beenackers, A. Pandit, Multiple-impeller systems with special emphasis on bioreactors: a critical review, Biochem. Eng. J. 6 (2000) 109–144.
[10] P. Vrabel, R. Van der Lans, K. Luyben, L. Boon, A. Nienow, Mixing in large-scale vessels stirred with multiple radial or radial and axial up pumping impellers: modelling and measurements, Chem. Eng. Sci. 55 (2000) 5881–5896.
[11] H. Barrué, J. Bertrand, B. Cristol, C. Xuereb, Eulerian simulation of dense solid-liquid suspension in multi-stage stirred vessel, J. Chem. Eng. Jpn. 34 (2001) 585–594.
[12] G. Montante, D. Pinelli, F. Magelli, Scale-up criteria for the solids distribution in slurry reactors stirred with multiple impellers, Chem. Eng. Sci. 58 (2003) 5363–5372.
[13] F. Guillard, C. Trägårdh, Mixing in industrial Rushton turbine-agitated reactors under aerated conditions, Chem. Eng. Process. 42 (2003) 373–386.
[14] H. Barrué, C. Xuereb, J. Bertrand, Comparison of multi-stage stirred vessels by a CFD approach: hydrodynamics, heat and mass transfer, Recent Res. Dev. Chem. Eng. 3 (1999) 107–120.
[15] A.D. Harvey III, S. Wood, D. Leng, Experimental and computational study of multiple impeller flows, Chem. Eng. Sci. 52 (1997) 1479–1491.
[16] M. Roustan, J.C. Pharamond, A. Liné, Agitation mélange: concepts théoriques de base, Techniques de l'ingénieur J3800 (1999).
[17] J. Ulbrecht, G. Patterson, Mixing of Liquids by Mechanical Agitation, Gordon and Breach Science Publishers, 1985.
[18] J. Aubin, Mixing capabilities of down-and up-pumping flow impellers in single phase and gas-liquid systems: experimental and CFD studies, Ph.D. Thesis, University of Sydney, Australia, and Institut National Polytechnique de Toulouse, France, 2001.
[19] P. Mavros, C. Baudou, Quantification of the performance of agitators in stirred vessels: definition and use of an agitation index, Chem. Eng. Res. Des. 75 (1997) 737–745.
[20] I. Houcine, E. Plasari, R. David, Effects of the stirred tank's design on power consumption and mixing time in liquid phase, Chem. Eng. Technol. 23 (2000) 605–613.
[21] J.M. Ottino, The Kinematics of Mixing: Stretching, Chaos and Transport, Cambridge University Press, Great Britain, 1989.
[22] Z.Z. Yang, L. ZhaoD, Preparation of bisphenol A epoxy resin waterborne dispersions by the phase inversion emulsification technique, Chin. J. Polym. Sci. 18 (2000) 33–38.